Morphological Stabilization of Polymer Photovoltaic Cells by Using Cross-Linkable Poly(3-(5-hexenyl)thiophene)

Shoji Miyanishi,[†] Keisuke Tajima,*[,†] and Kazuhito Hashimoto*[,†,‡]

Department of Applied Chemistry, School of Engineering, The University of Tokyo, 7-3-1 Hongo, Bunkyo-ku, Tokyo 113-8656, Japan, and HASHIMOTO Light Energy Conversion Project, ERATO, Japan Science and Technology Agency (JST), Tokyo, Japan

Received December 22, 2008

ABSTRACT: A new cross-linkable regioregular poly(3-(5-hexenyl)thiophene) (P3HNT) was synthesized via the Grignard metathesis route for the purpose of stabilizing the film morphology in polymer photovoltaic cells. Bulk heterojunction photovoltaic cells with P3HNT and (6,6)-phenyl C_{61} butyric acid methyl ester (PCBM) showed initial power conversion efficiency comparable to that of cells with poly(3-hexylthiophene) (P3HT) due to the high crystallinity of the polymer in the films. P3HNT underwent cross-linking at the vinyl groups of the side chains upon a thermal treatment, which was confirmed by the insolubility of the films in organic solvents and by their thermal behavior. As a result, the formation of large aggregations of PCBM was prevented in P3HNT:PCBM films even after prolonged thermal annealing. In addition, the deterioration of the photoconversion performance was suppressed in the polymer photovoltaic cells compared to cells with noncross-linkable P3HT:PCBM.

Introduction

Electronic devices based on conjugated polymers, such as light emitting diodes (LEDs), field effect transistors (FETs), and photovoltaic cells (PV cells), have started to draw considerable attention recently as a result of their high potential for the fabrication of low cost, large-area devices on flexible substrates by simple means of painting or printing from polymer solutions. Due to the soft nature of the organic materials, however, these devices generally suffer from morphological instabilities, such as crystallization or phase separation of the materials inside the films, which can lead to the deterioration of the device performance.[1−5] In addition, the solution processes of conjugated polymers present a difficulty for the fabrication of multilayered structures by repeated coatings since the solvent for the second layer destroys the first organic layer underneath. Since multilayer structures are often important in many organic electronic devices for controlling the flow of the charge carriers in the films,[6,7] this difficulty is one of the serious problems obstructing the exploration of optimal device structures. In this regard, the use of cross-linkable conjugated polymers has been proposed for the purpose of overcoming these disadvantages.[8−19] For example, Li et al. reported a thermally cross-linkable oligofluorene for organic LED application to improve the thermal and morphological stability of the devices.[17] Meerholz et al. synthesized cross-linkable hole transport materials for use in polymer LEDs.[13] The film of these materials can undergo photochemical cross-linking and become insoluble to organic solvents, which allows for multiple layers to be introduced on the material by subsequent coating.

Polymer PV cells share both the advantages and the shortcomings described above, although the materials and the structures are different from those of polymer LEDs or FETs. The most commonly used structure is a bulk heterojunction, which is a physical mixture of donor and acceptor materials.[20,21] Recent research has suggested that controlling the phase separation of the donor and the acceptor in films smaller than the exciton diffusion length of the material (typically ∼10 nm) is of high importance for achieving highly efficient charge separation and transport.[22−24] Especially in the case of the combination of poly(3-hexylthiophene) (P3HT) and (6,6)-phenyl C_{61} butyric acid methyl ester (PCBM), thermal annealing of the films has been used to control this phase separation.[25] During the thermal annealing, both the polymer and PCBM crystallize to form a nanoscale interpenetrating network which drastically enhances the device performance.[26] However, even if such a phase-separated nanostructure is constructed, this morphology is not thermally stable and may gradually undergo changes during the device operation since the polymer and the PCBM thermodynamically prefer to segregate from each other.[27,28] In fact, it was reported that a prolonged thermal treatment induces the formation of large aggregations of PCBM in the films, and as a result the device performance was drastically lowered by this notable morphological change.[29−33] Therefore, morphology control which only depends on thermal annealing might be insufficient for achieving a stable and reliable mixing morphology of the donor and the acceptor. In order to suppress the PCBM aggregation, Gaudiana et al. synthesized cross-linkable fullerene derivatives containing glycidyl functionality.[34,35] They succeeded in suppressing the large aggregation of the fullerene derivative under thermal annealing after acid-catalyzed cross-linking. However, the PV performance of the cells was much lower in comparison to the corresponding donor/acceptor system. To the best of our knowledge, there has been no report on the utilization of the cross-linkable conjugated polymers for the purpose of controlling the morphology in the polymer PV cells.

In this work, we synthesized a new cross-linkable regioregular poly(3-(5-hexenyl)thiophene) (P3HNT) (Schemes 1 and 2). Although there are many choices for the reactive functional groups, we adopted a vinyl group at the end of the side chain as the cross-linkable site in this study. The reason for this choice is 2-fold. The first is to maintain the high crystallinity of the polymer. In the poly(3-alkylthiophene)s films, the $\pi-\pi$ stacking of the polymers is largely affected by the packing of the side chains.[36,37] The introduction of large functionalities to the side chains can result in the decrease of crystallinity, thereby

* Corresponding authors. E-mail: (K.T.) k-tajima@light.t.u-tokyo.ac.jp; (K.H.) hashimoto@light.t.u-tokyo.ac.jp.
[†] Department of Applied Chemistry, School of Engineering, The University of Tokyo.
[‡] HASHIMOTO Light Energy Conversion Project, ERATO, Japan Science and Technology Agency (JST).

10.1021/ma802839a CCC: $40.75
Published on Web 02/04/2009

Scheme 1. Synthetic Route for the Monomer of P3HNT

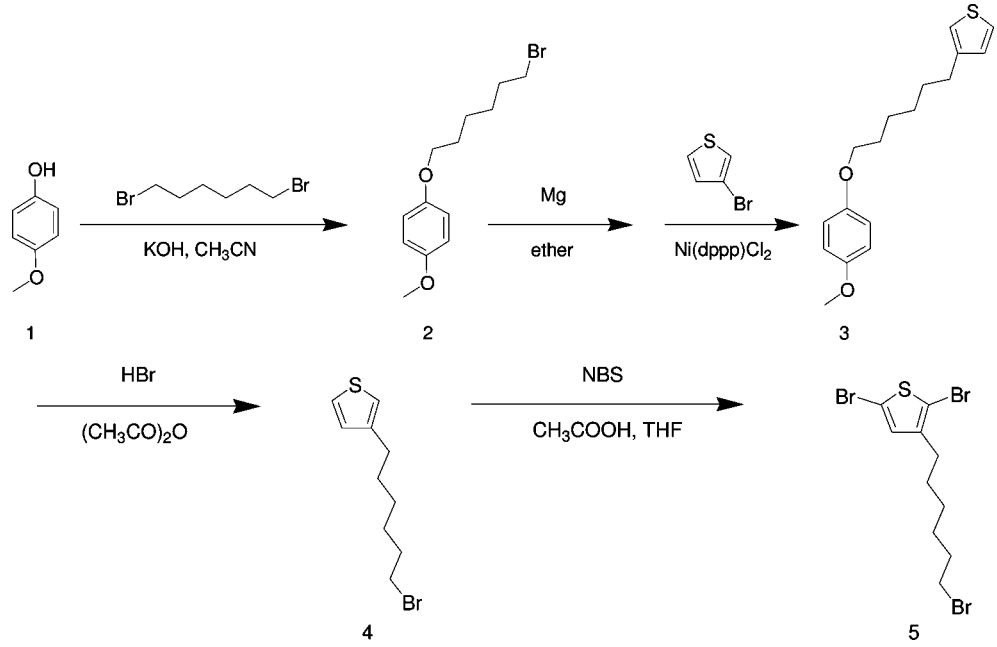

Scheme 2. Polymerization and Side Chain Conversion Reactions for the Synthesis of P3HNT

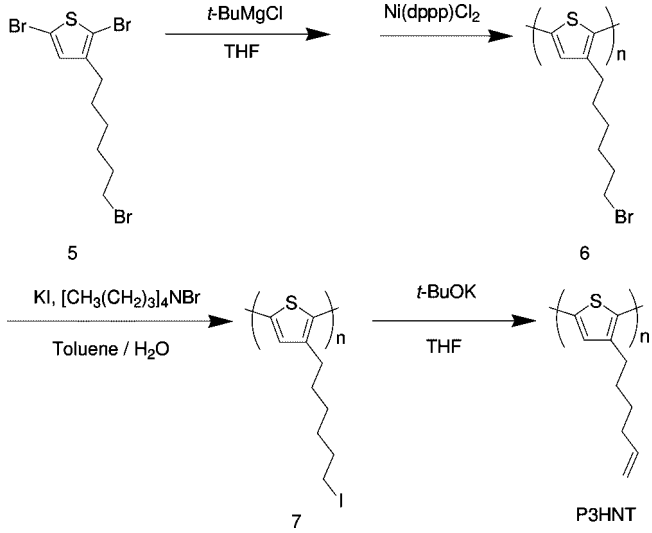

decreasing the hole mobility in the polythiophene main chains.[38] In order to achieve high crystallinity of the polymer, it is desirable that the side chain of the cross-linkable polymer is as close as possible to the linear alkyl group. Furthermore, the second reason for choosing vinyl groups is to induce the cross-linking reaction without adding an initiator. In general, the mixing of materials irrelevant to energy conversion into the active layer can have undesirable effects on the photoconversion, such as the formation of charge trapping sites, resulting in lower performance. Therefore, a thermally initiated radical reaction of vinyl groups without using an initiator is considered suitable for application in actual devices. After thermal treatment, P3HNT is expected to crystallize and generate nanoscale phase-separated structures in a manner similar to the case of P3HT:PCBM films due to their structural similarity. At the same time, the thermal treatment induces a cross-linking reaction of the vinyl group at the side chains. After the process of cross-linking is complete, the diffusion of PCBM into the film can be lowered in order to suppress the formation of large aggregations. As a result, we can expect the thermal stability of the cells to improve in comparison to noncross-linkable P3HT:PCBM bulk heterojunction.

Results and Discussion

Monomer Synthesis. The synthetic route for the monomer of P3HNT is shown in Scheme 1. 1-[(6-Bromohexyl)oxy]-4-methoxybenzene (**2**) was synthesized from 4-methoxyphenol (**1**) by Williamson etherification. Note that the residue of unreacted 1,6-dibromohexane must be carefully removed at this stage by vacuum distillation and subsequent repeated recrystallization since it can react in the next step to produce an impurity. 3-[6-(4-Methoxyphenoxy)hexyl]thiophene (**3**) was synthesized by using the nickel-catalyzed Kumada−Tamao−Corriu coupling with the Grignard product of **2** and 3-bromothiophene. 3-(6-bromohexyl)thiophene (**4**) was synthesized from **3** by using hydrogen bromide. Finally, 2,5-dibromo-3-(6-bromohexyl)thiophene (**5**) was obtained by dibromination of **4** with NBS.

McCullough et al. reported a simpler synthetic route for **5**, in which **4** was synthesized from 3-bromothiophene and 1,6-dibromohexane in one step.[39] However, we experienced difficulties removing the byproduct (possibly 2-(6-bromohexyl)thiophene) from **4** by vacuum distillation. It was found that the byproduct was incorporated into the polymer chain in the following step. As a result, the absorption and the crystallinity of the product polymer were significantly lowered in comparison to the impurity-free regioregular P3HNT even when the amount of the impurity was very small (less than 3% as determined by ^{1}H NMR). Therefore, we adopted the synthetic route for **4** reported by Heid et al. to avoid this problem.[40]

Polymerization. The polymer **6** was synthesized by following the method reported by McCullough et al.[39] (Scheme 2). After the polymerization, the reaction mixture was quenched with 5 M HCl, following the report by Yokozawa et al.[41] This quenching procedure prevents the polymers from undergoing dimerization in order to maintain the narrow molecular weight distribution while efficiently removing the inorganic impurities from the product. The number-averaged molecular weight (M_n) and the polydispersity index (M_w/M_n) of this polymer were 32000 and 1.30, respectively, as determined by GPC. The regioregularity of this polymer was more than 97%, which was

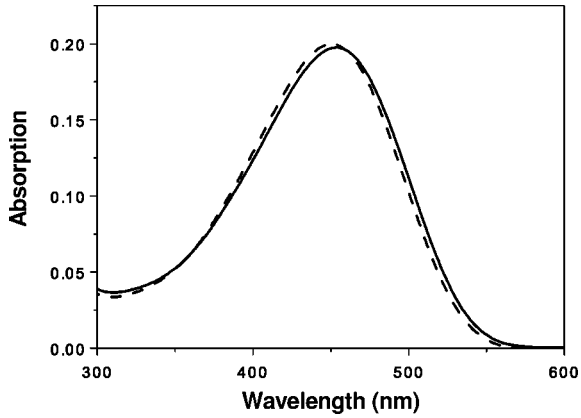

Figure 1. UV−vis absorption spectra of P3HT (solid) and P3HNT (dashed) in $CHCl_3$ solution (4 mg L^{-1}).

confirmed by the peak integrations of ^{1}H NMR.[42] After the polymer purification was complete, the bromide groups at the end of the side chains in polymer **6** were converted into iodide groups to produce polymer **7** (Scheme 2). The iodide groups in polymer **7** were converted into vinyl groups by treatment with *t*-BuOK to obtain P3HNT. It was confirmed by ^{1}H NMR spectrum that 98% of iodide groups were converted into vinyl groups and 2% were converted into *tert*-butyl ether groups.

As a control material for P3HNT, we also synthesized P3HT by following a similar method (see the Supporting Information).[43] It was confirmed with ^{1}H NMR that the regioregularity of P3HT is similar to that of P3HNT (more than 97%). M_n of the P3HT was 42600 with $M_w/M_n = 1.18$, as determined by GPC.

Polymer Characterizations. *Absorption Spectra.* The absorption spectrum of P3HNT in $CHCl_3$ is almost identical to that of P3HT, as shown in Figure 1. The peak tops of P3HT and P3HNT absorption are at 453 and 451 nm, respectively, which shows that the conjugation length of the main chain in the solution was not affected by the introduction of vinyl groups at the side chains. The peak tops of the absorption spectra of the films spin-coated with both P3HT and P3HNT underwent red shifts to 560 nm in comparison to those in the solutions, with similar absorption shoulders around 600 nm (Figure 2a). These changes indicate the extension of the π-conjugation lengths and the interchain interaction between the polythiophene backbones in the films.[44] Similar peak shifts and the formation of shoulders were also observed in the films coated with the mixture of the polymers and PCBM (polymer:PCBM = 1.0:0.8 by weight) (Figure 2b). These similarities in the absorption spectra indicate that P3HNT is characterized by strong intermolecular interactions, similarly to P3HT in the films.

X-ray Diffraction (XRD) Measurements. Figure 3 shows the XRD patterns of the bulk samples of P3HT and P3HNT. Both samples show diffraction peaks at low angles, which can be attributed to a lamellar structure typically observed in crystalline regioregular P3HT.[45,46] The *d*-spacings of the diffraction from (100), (200) and (300) are 16.5, 8.40 and 5.39 Å for P3HT and 16.5, 8.08 and 5.25 Å for P3HNT, respectively. A strong broad peak was also observed at 3.86 Å for P3HT and at 3.80 Å for P3HNT, which correspond to the $\pi-\pi$ stacking distance between the polythiophene chains. The XRD results indicate that P3HNT adopts a crystalline lamellar structure with an interlayer and an interchain distance very similar to P3HT.

Photoelectron Yield Spectroscopy (PYS) Measurements. The ionization potentials (IPs) of the synthesized polymers were determined from the onset potentials of the photoelectrons by PYS measurements performed on the films (see Supporting Information). The results are summarized in Figure 4 as a function of the annealing time at 150 °C. It was found that the IPs of P3HNT were larger than those of P3HT by ca. 0.1 eV both in the pristine polymer films and in the mixture films with PCBM. The IPs of the films were not considerably changed after the thermal annealing at 150 °C. Considering the results in the previous sections, in which the optical properties and the crystal structures are quite similar between P3HT and P3HNT, this difference in IPs is somewhat unexpected. We assume that the larger IPs in P3HNT are due to small differences in the conformations and/or the packing of the polythiophene main chains as compared to P3HT.

Evaluation of the Cross-Linkability of the Polymers. *UV−Vis Spectra Measurements.* The cross-linkablility of P3HNT by thermal annealing was investigated by the insolubility of the film in organic solvents as monitored by UV−vis absorption spectra. Namely, thin films of the pristine polymers and the polymer:PCBM mixture films were prepared by spin-coating on quartz substrates, which were subsequently annealed at 150 °C for 2 h under N_2 atmosphere. After the UV−vis spectra of the samples were measured, the films were immersed into $CHCl_3$ for 20 min. After the samples were dried, the UV−vis spectra were measured again in order to check the amount of polymers remaining on the substrates. Figure 5 shows the UV−vis spectra of the pristine polymer films before and after the solvent immersion. In the P3HT film, no absorption was observed after the immersion, indicating that P3HT was completely dissolved into $CHCl_3$ (Figure 5a). On the other hand, about half of the absorption of P3HNT still remained after the same treatment (Figure 5b). This result indicates that the polymer was cross-linked at the side chains by the thermal annealing and thus became insoluble in organic solvents. Furthermore, the amount of insoluble parts of the cross-linked polymer increased together with the annealing time (see Supporting Information).

Similar insolubility of P3HNT was also observed in the polymer:PCBM mixture films (Figure 6). The absorption of both P3HT and PCBM disappeared completely in the P3HT:PCBM film after the immersion into $CHCl_3$ (Figure 6a). In contrast, the absorption of the polymer in P3HNT:PCBM film remained after the immersion, while that of PCBM at 335 and 264 nm disappeared completely, suggesting the extraction of PCBM from the film (Figure 6b). These results indicate that P3HNT was thermally cross-linkable even in the mixture films coated with PCBM.

FT-IR Measurements. The conversion of the vinyl groups in P3HNT during the thermal annealing was directly monitored with FT-IR. Figure 7 shows the changes in the FT-IR spectra of P3HNT film drop-cast on KBr in the region of the out-of-plane bending vibration of the C=C bond (909 cm^{-1}). The sample was fixed in the FT-IR measurement system and was thermally annealed *in situ* under N_2 atmosphere. The intensity of the vinyl group was reduced by ca. 4% after annealing at 150 °C for 24 h. This low conversion of the vinyl groups can be explained by the crystalline nature of the P3HNT, which might reduce the mobility of the side chains and the reactivity. Nevertheless, the insolubility as inferred from the UV−vis results in the previous section indicates that this small conversion of the vinyl groups (less than 4%) entailed drastic changes in the properties of the polymer, such as solubility and physical mobility, even after thermal annealing for 1 h.

Differential Scanning Calorimetry (DSC) Measurements. Figure 8 shows the DSC traces of P3HT and P3HNT. The thermal cycles were repeated and the traces were superimposed from the second cycles. P3HT underwent melting at 237 °C and recrystallization at 207 °C, as reported previously for

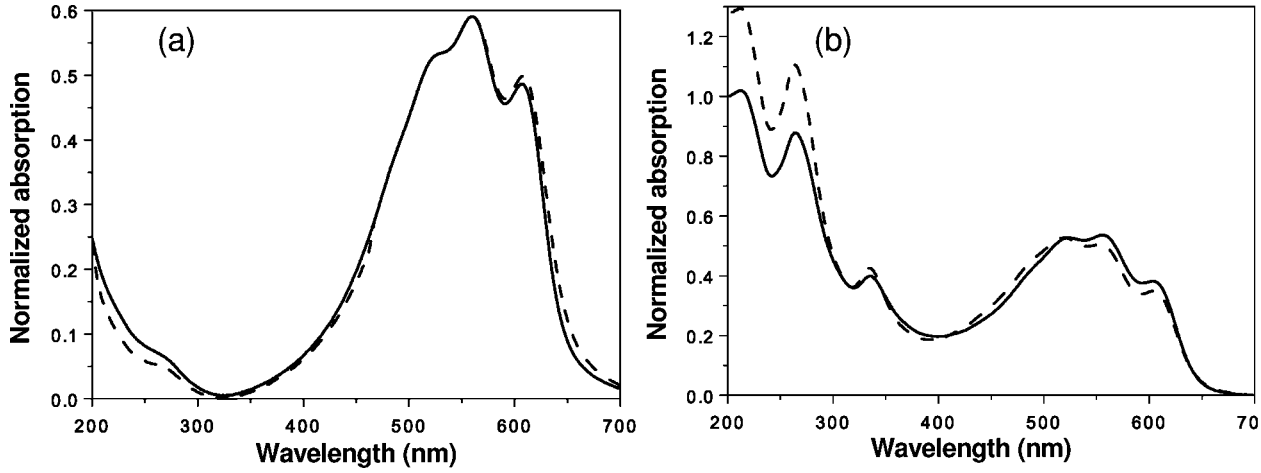

Figure 2. UV−vis absorption spectra of the spin-coated films after 5 min of annealing at 150 °C for (a) P3HT (solid) and P3HNT (dashed) and (b) bulk heterojunction films of P3HT:PCBM (solid) and P3HNT:PCBM (dashed). Polymer:PCBM = 1.0:0.8 (by weight).

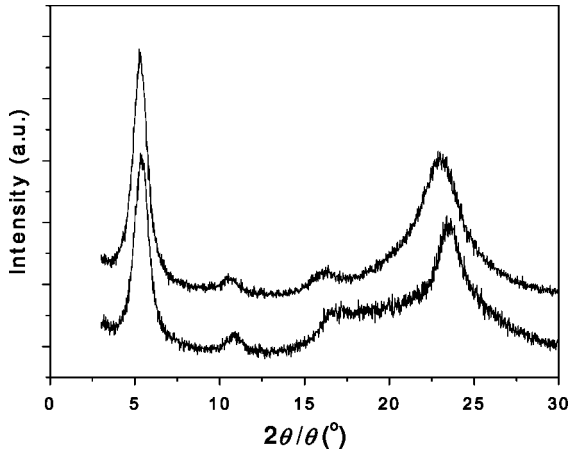

Figure 3. XRD patterns of the bulk samples of P3HT (top) and P3HNT (bottom).

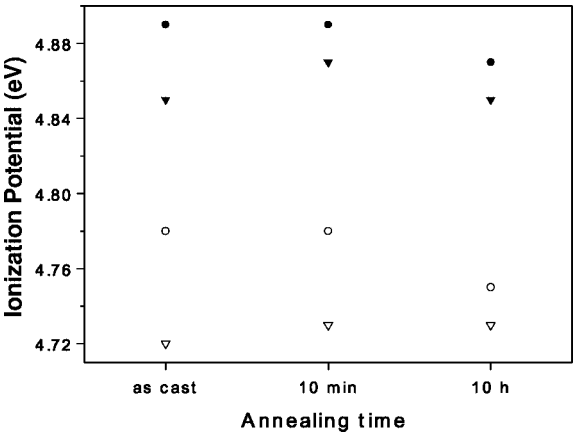

Figure 4. Ionization potentials of the polymer films as measured by PYS plotted against the annealing time at 150 °C for P3HT (open circles), P3HT:PCBM (open triangles), P3HNT (closed circle), and P3HNT:PCBM (closed triangles). Polymer:PCBM = 1.0:0.8 (by weight).

regioregular P3HT.[45] The intensities and the positions of the peaks did not change in the repeated thermal cycles. Furthermore, P3HNT underwent melting at 224 °C and recrystallization at 188 °C in the second cycle. In contrast to P3HT, the intensities of both peaks of P3HNT decreased, and the positions were shifted to lower temperatures in the repeated thermal cycles. This change in thermal behavior can be attributed to the cross-linking reaction during the measurement cycles. The molten polymers are expected to undergo faster cross-linking reaction at temperatures above the melting point due to the higher mobility of the side chains. During the cooling process, the cross-linked fractions can prevent the alkyl side chains from undergoing interchain packing, resulting in lowered peak intensity after the repetition of the thermal cycles. In addition, the cross-linkable fraction can induce the strain and reduce the molecular interaction in the crystalline phase, which can shift the melting and recrystallization peaks to lower temperatures during the cycles.

Application to Photovoltaic Cells. *Initial Device Performance.* Table 1 shows the performances of bulk heterojunction PV devices with P3HT or P3HNT combined with PCBM after thermal annealing at 150 °C for 5 min. Note that this short annealing time does not induce significant cross-linking of the vinyl groups, which is confirmed by the solubility of the films in $CHCl_3$. The devices with P3HNT showed a smaller averaged value of I_{SC}, a comparable FF and a higher V_{OC} in comparison to those with P3HT (Figure 9). As a result, the power conversion efficiency (PCE) of the P3HNT device was comparable to that of P3HT. As shown in the previous sections, P3HNT has an absorption profile and high crystallinity similar to P3HT, which might contribute to the high performance observed when it is combined with P3HNT since the crystallinity of the polymer is known to have a notable effect on the device performance. It has been proposed that the maximum V_{OC} achievable in the bulk heterojunction is determined by the difference of the LUMO level of the acceptor and the HOMO level of the donor.[47−49] The higher V_{OC} in P3HNT can be explained by the larger IP in comparison to that of P3HT (see Figure 4). It is noteworthy that the higher V_{OC} of the devices was induced by the very small modification of the polymer side chains. Detailed investigation can provide an insight into the polymer design necessary for the improvement of V_{OC} in the polymer PV cells.

Overall, P3HNT:PCBM gave a good initial device performance comparable to that of P3HT:PCBM, which enables us to evaluate the long-term thermal stability of the devices in the following sections.

Long-Term Thermal Stability of the Devices. Bulk heterojunction devices comprising P3HT and P3HNT were fabricated simultaneously and were subsequently annealed at 150 °C in a glovebox filled with N_2 (water <0.1 ppm and O_2 < 0.2 ppm) as an accelerated test for device stability. P3HNT was cross-linked in the bulk heterojunction films during this long-thermal annealing process, which was confirmed by the

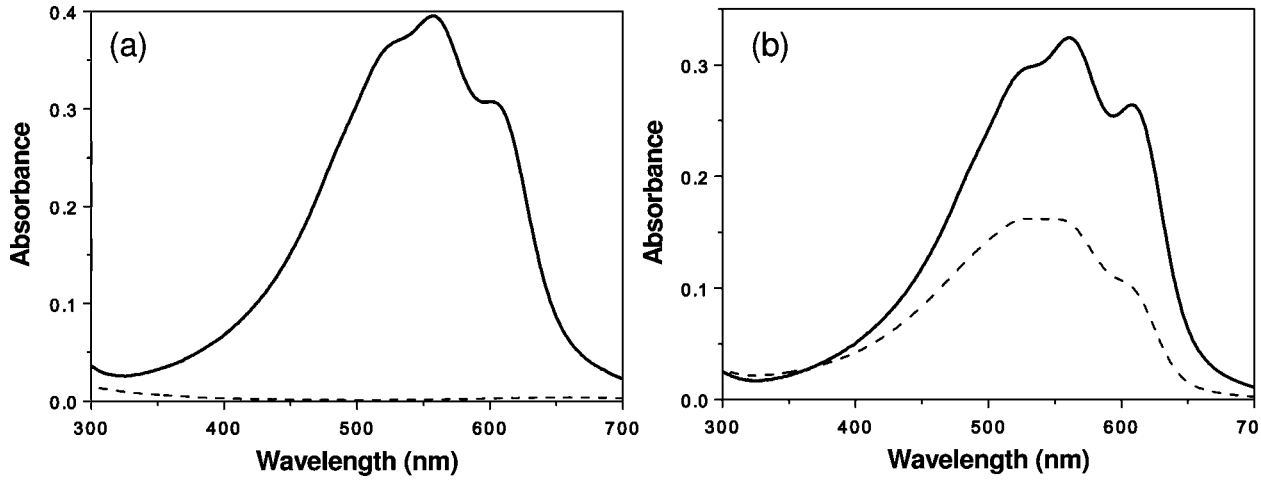

Figure 5. UV−vis absorption spectra of thermally annealed (a) P3HT and (b) P3HNT films before (solid) and after (dashed) the immersion into $CHCl_3$.

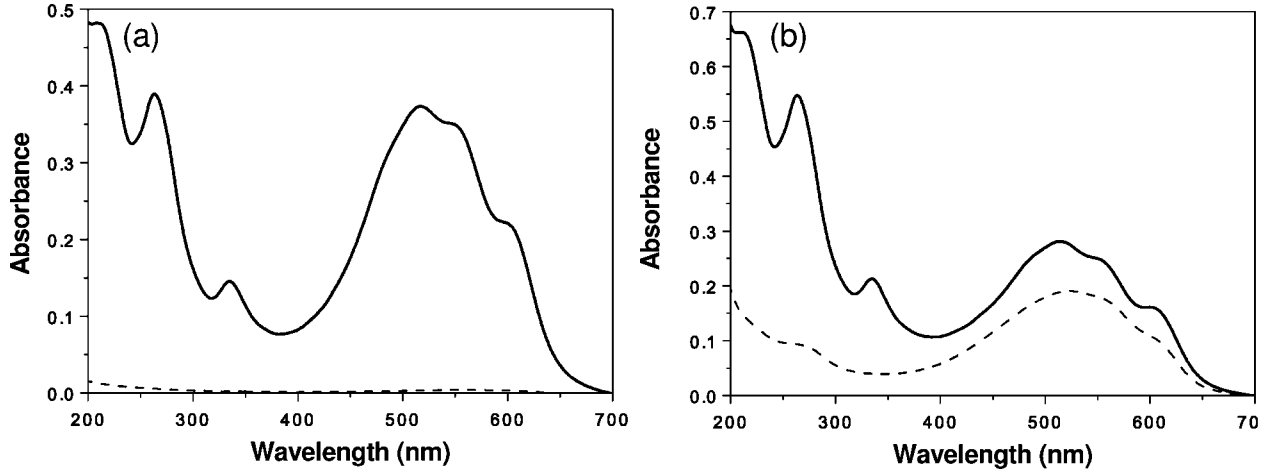

Figure 6. UV−vis absorption spectra of thermally annealed (a) P3HT:PCBM and (b) P3HNT:PCBM films before (solid) and after (dashed) the immersion into $CHCl_3$. Polymer:PCBM = 1.0:0.8 (by weight).

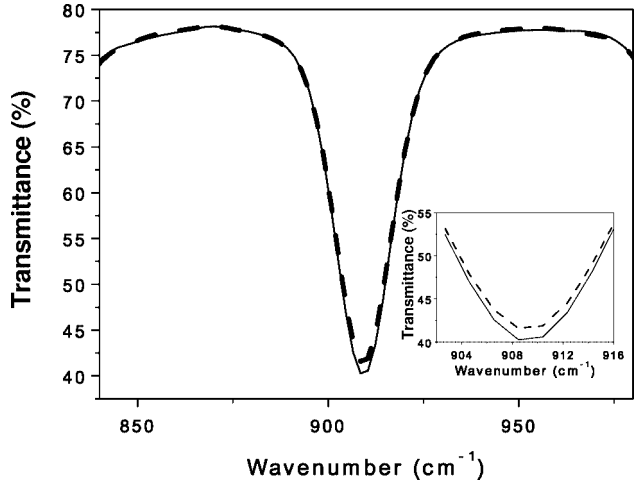

Figure 7. FT-IR absorption spectra of the P3HNT film before (solid) and after (dashed) the annealing at 150 °C for 24 h.

insolubility of the film in $CHCl_3$. Figure 10 shows the device parameters plotted against the annealing time with standard deviations. Both devices showed similar averaged initial PCEs of ca. 3%. In the course of the thermal annealing, all the averaged device parameters decreased in the case of P3HT: V_{OC} from 0.54 to 0.46 V (−15%), FF from 0.65 to 051 (−22%), and I_{SC} from 8.93 to 4.22 mA cm^{-2} (−53%) after annealing for 600 min (changes relative to the start value are in parentheses). As a result, PCE decreased from 3.11% to 1.00%. Moreover, the deviation of the parameters became larger as the annealing progressed. The device comprising P3HNT, however, showed a completely different tendency: V_{OC} increased slightly from 0.64 to 0.69 V (+7.1%), FF decreased from 0.63 to 0.43 (−31%), while the decrease of I_{SC} was significantly suppressed in comparison to the P3HT devices (from 7.55 to 5.83 mA cm^{-1} (−23%)) after annealing for 600 h. As a result, the deterioration of PCE was suppressed with P3HNT (from 3.03% to 1.74%) in comparison to P3HT devices. In addition, the deviations of the device parameters were smaller than those in the P3HT devices in the course of the annealing.

Morphological Changes During the Thermal Annealing. Figure 11 shows optical micrographic images of the bulk heterojunction films in the devices after the annealing. The observed areas are not covered by Al electrodes. It was clearly observed that large aggregations of PCBM appeared everywhere in P3HT:PCBM films after annealing for 2 h, and they grew to larger needle-shape crystals as the annealing progressed to 10 h (Figure 11a). Similar aggregations were observed in the area covered with Al electrodes visible as reflective bumps on the surface (Figure 12a). This large aggregation and crystallization of PCBM has been previously reported.[24,28,50] In striking contrast, only a small amount of PCBM aggregation was observed in P3HNT:PCBM films even after 10 h of annealing,

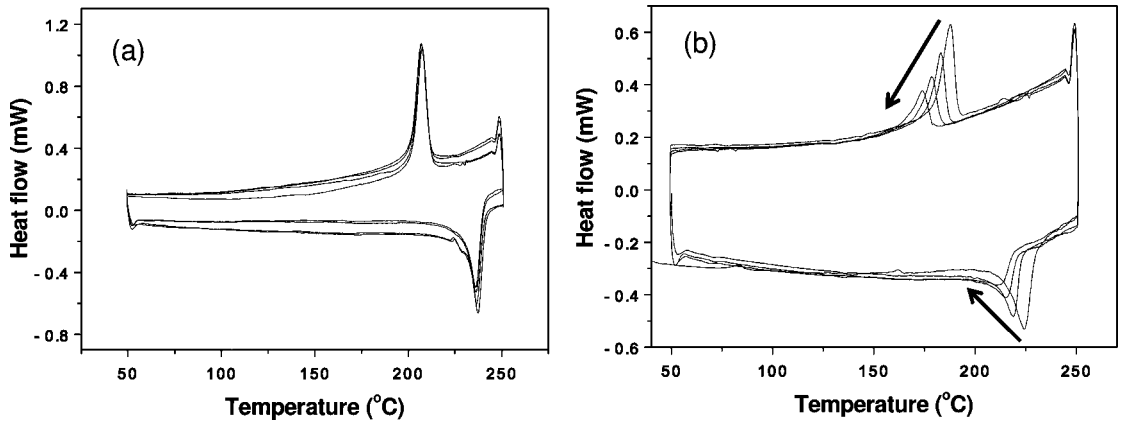

Figure 8. DSC traces of (a) P3HT (b) P3HNT. Cycles 2−5 are superimposed. Arrows in part b indicate the direction of the change during the repeated cycles.

Table 1. Summary of Initial Device Performance with the Synthesized Polymers[a]

synthesized polymers	I_{SC} (mA cm^{-2})	V_{OC} (V)	PCE[b] (%)	FF
P3HT	8.78	0.56	3.33	0.677
P3HNT	7.61	0.64	3.16	0.648

[a] Polymer:PCBM = 1.0:0.8 (by weight). [b] Post annealing after Al deposition at 150 °C for 5 min. Measurement was conducted under irradiation of AM1.5 (100 mW cm^{-2}).

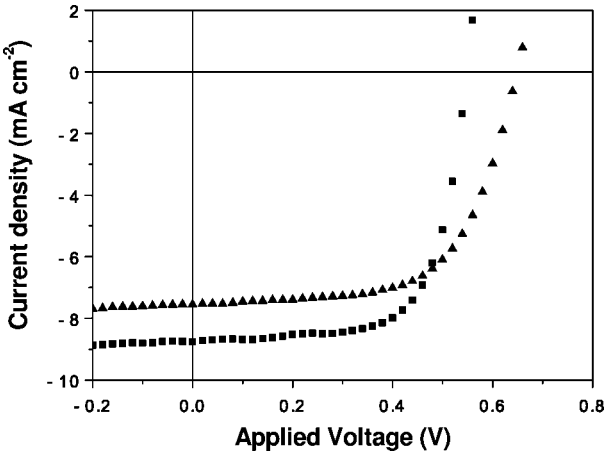

Figure 9. Initial $I-V$ curves of the devices with P3HT (squares) and P3HNT (triangles) combined with PCBM.

as shown in Figure 11b. The surface of the Al electrodes was flat, and no sign of large PCBM aggregation was observed beneath the Al after the thermal annealing, as shown in Figure 12b. From these observations, we concluded that the large aggregation of PCBM in the films was suppressed by the cross-linking of P3HNT during the thermal annealing.

To investigate the morphological change in smaller scale, atomic force microscopy (AFM) images of the polymer:PCBM films were taken after various annealing time. The points of the observation were selected to avoid the large PCBM aggregations if they existed. The AFM height images of P3HT:PCBM film initially showed a flat surface with R_a of 1.4 nm, but the surface became rougher after 1 h annealing with R_a of 3.6 nm (see Supporting Information). This change of the morphology could be attributed to the phase separation and crystallization of the P3HT and PCBM in nanoscale. In contrast, P3HNT:PCBM film showed no clear difference in the surface morphology with a constant R_a of about 1.4 nm even after the prolonged annealing. These AFM observations also suggest less significant morphological change in nanoscale for P3HNT:PCBM due to the cross-linking reaction of the polymer.

Discussion on the Performance Change During the Thermal Annealing. The performance deterioration in P3HT:PCBM bulk heterojunction PV cells might be the result of the combination of several factors, such as changes in the layer interfaces, degradation of the organic materials, oxidation of the electrode metals, changes in the mixing morphology, etc. The contribution of each factor is likely to have strong dependence on the experimental conditions adopted for the stability evaluation, which makes it difficult to single out a generalized main factor for the device deterioration. In our accelerated experimental conditions at 150 °C, i.e., above the glass transition temperature of the polymers, the high physical mobility of the polymers allows PCBM to diffuse inside the films, and thus the changes in the mixing morphology might be a strong factor in the device deterioration process. The formation of large PCBM aggregations in the P3HT:PCBM film can reduce the interface of the donor and the acceptor, which can lead to a low charge separation efficiency. The rapid decrease of I_{SC} in the P3HT:PCBM devices can be explained by this morphological change induced by the thermal treatment. Furthermore, the formation of large PCBM aggregations might damage the interfacial structure between the organic active layer and the Al electrode (see Figure 12a), which can also contribute to the gradual decrease of V_{OC} and FF in the P3HT:PCBM devices by decreasing the shunt resistance of the devices. This morphological change can also induce larger fluctuations in the device performance during the thermal treatment.

In contrast, the P3HNT:PCBM films did not show a large phase separation between the components due to the cross-linking reaction of P3HNT. AFM observations also support the stabilization of the local mixing morphology in P3HNT:PCBM. This can lead to a more stable I_{SC} and smaller deterioration of the device performance in comparison to those of P3HT:PCBM devices. Since I_{SC} was still decreased with P3HNT, other deterioration paths described above should also be investigated to achieve the higher device stability. Nevertheless, it was clearly demonstrated that the cross-linking of the semiconducting polymer stabilized the mixing morphology of the films, which as a result improved the thermal stability of the polymer PV in comparison to the conventional system. The slight increase in V_{OC} and the faster decrease in FF in the case of P3HNT are not fully understood yet. One possibility is that the cross-linking reaction at the side chains can cause strain in the polymer backbone to change the conformation and/or the stacking manner that can affect V_{OC} and FF. Further investigation on the charge mobility of the polymers during the cross-linking reaction is necessary to clarify these effects.

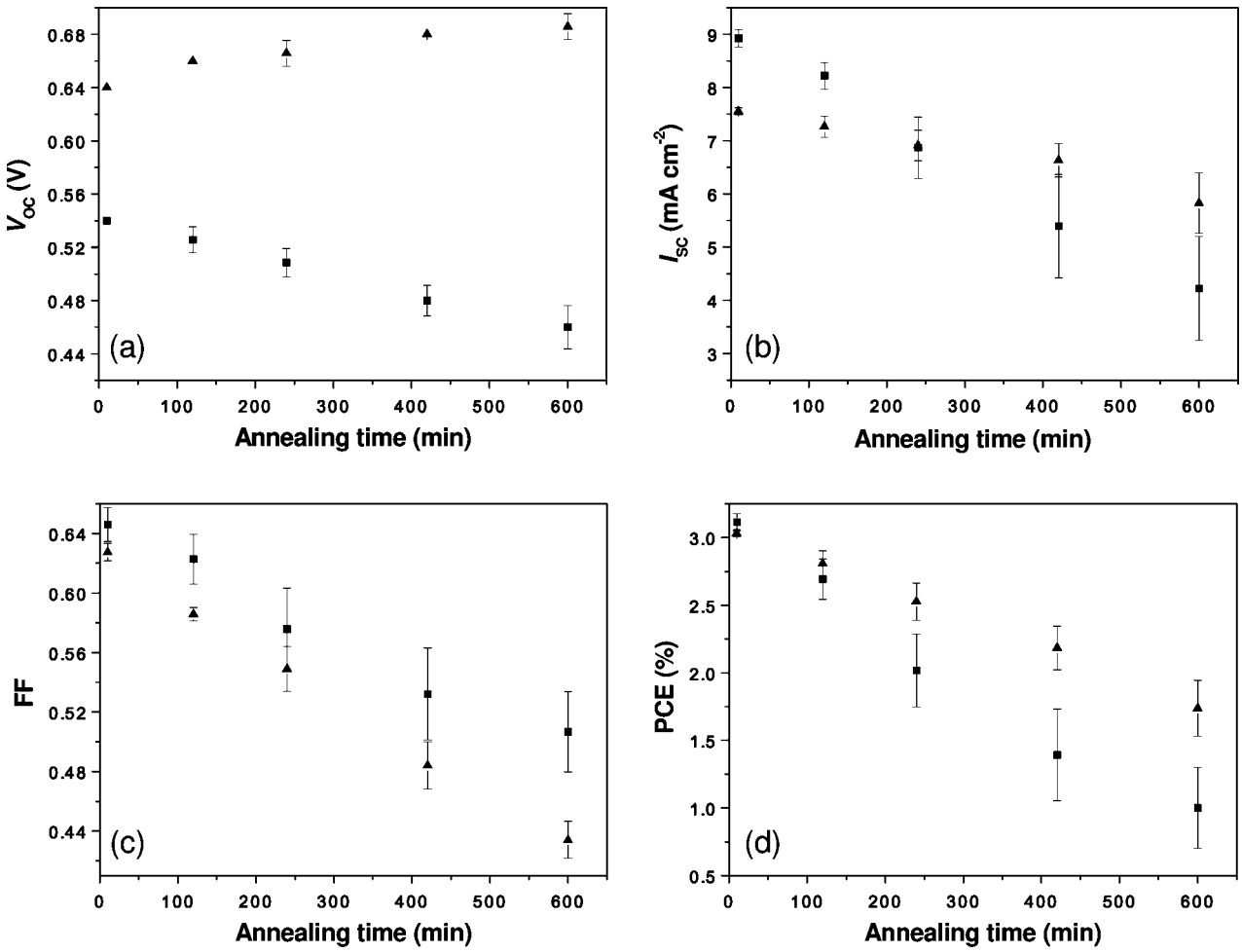

Figure 10. Device performance of P3HT:PCBM (squares) and P3HNT:PCBM (triangles) during thermal annealing at 150 °C. (a) V_{OC} (b) I_{SC} (c) FF, and (d) PCE.

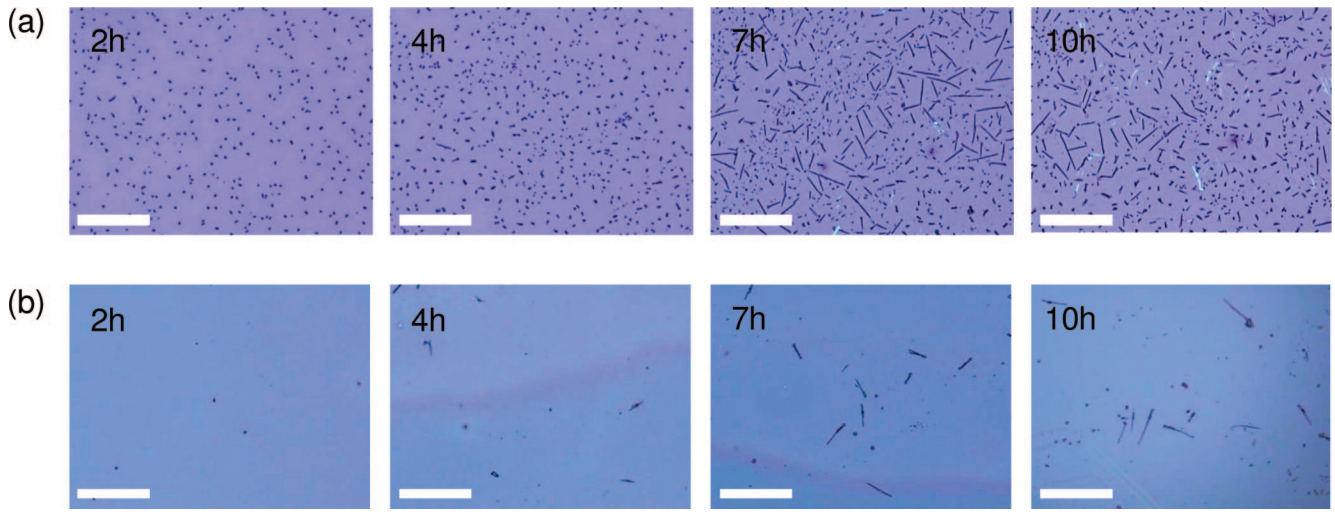

Figure 11. Optical microscope images of (a) P3HT:PCBM (b) P3HNT:PCBM films after thermal annealing at 150 °C. Annealing times are presented in the images (scale bar: 200 μm).

Conclusion

We synthesized a new cross-linkable regioregular P3HNT. The initial device performance in the case of P3HNT after the short thermal annealing is comparable to that of P3HT due to the high crystallinity of the polymer. After a prolonged thermal treatment, the formation of large PCBM aggregations was suppressed by the cross-linking of the polymer, which led to a more stable device performance in the case of P3HNT as compared to that of P3HT. To our knowledge, this is the first report on the utilization of cross-linkable conjugated polymers for the stabilization of the morphology and the device performance in polymer PV cells. The current approach might be useful for the development of stable polymer PV cells. The insolubility of the cross-linkable P3HNT is also considered to be useful for the formation of multilayers by subsequent wet-coating processes, which can enable the fabrication of efficient multilayer or tandem PV cells.

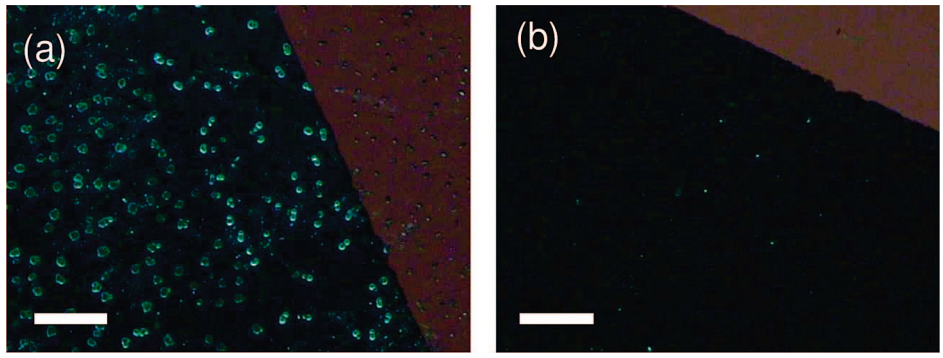

Figure 12. Optical microscope images of the device surface after 10 h of thermal annealing (dark areas in the images are covered by the Al electrode) (a) P3HT:PCBM and (b) P3HNT:PCBM (scale bar: 100 μm).

Experimental Section

Synthesis. All reagents are used as received from the manufacturer. 3-[6-(4-Methoxyphenoxy)hexyl]thiophene (**3**) and 3-(6-bromohexylthiophene) (**4**) were synthesized as reported by Heid et al.[40] 2,5-dibromo-3-(6-bromohexyl)thiophene (**5**) was synthesized as reported by McCullough et al.[39]

1-(6-Bromohexyl)-4-methoxybenzene (2). 4-Methoxyphenol (**1**) (51.3 g, 0.41 mol), KOH (31 g, 0.55 mol), 18-crown-6 (500 mg 1.9 mmol), and MeCN (1000 mL) were added to a three-necked 2 L round-bottom flask equipped with a large magnetic stirring bar. After the compounds were dissolved, 1,6-dibromohexane (200 g, 0.82 mol) was added into the reaction solution. After the reaction mixture was refluxed overnight, it was filtered to remove the KBr. MeCN was evaporated and the compound was redissolved in hexane. The solution was sequentially washed with 2 M NaOH (aq), 1 M NaCl (aq), and then twice with water. After evaporating the hexane, the unreacted 1,6-dibromohexane was removed by vacuum distillation. The residue was redissolved in hexane and cooled down for recrystallization. The product was filtered and washed using cold hexane. This procedure was repeated for several times in order to obtain pure product **2** (68.5 g, 0.24 mol) in a 58% yield. ^{1}H NMR (500 MHz, $CDCl_3$): 6.86 (s, 4H), 3.92 (t, 2H), 3.77 (s, 3H), 3.42 (t, 2H), 1.90 (m, 2H), 1.77 (m, 2H), 1.51 (m. 4H).

Poly[3-(6-bromohexyl)thiophene] (6). 2,5-Dibromo-3-(6-bromohexyl)thiophene (**5**) (2.5 g, 6.2 mmol) and 50 mL of anhydrous THF were added to a two-necked 100 mL round-bottom flask equipped with a stirring bar. *t*-BuMgCl (2.0 M in diethyl ether, 3.1 mL, 6.2 mmol) was then added to the flask with a syringe. After the solution was heated to reflux and stirred for 2 h, the heating bath was removed and Ni(dppp)Cl_2 (18.4 mg, 0.034 mmol) was added. The mixture was stirred for 1.5 h at room temperature, after which the reaction solution was quenched with 5 M HCl. The polymer was extracted with $CHCl_3$ and sequentially washed with 1 M HCl aq., saturated $NaHCO_3$ aq., and water. After the solution was dried with $MgSO_4$ and the $CHCl_3$ was evaporated, the residue was precipitated into MeOH. After filtration, the polymer was sequentially purified with MeOH and hexane by Soxhlet extraction. The polymer was extracted with $CHCl_3$ and reprecipitated into MeOH. The suspension was filtered, and the residue was dried in vacuum to give 762 mg of product **6** in 50% yield. ^{1}H NMR (500 MHz, $CDCl_3$): 6.98 (s, 1H), 3.43(t, 2H), 2.82 (t, 2H), 1.90 (m, 2H), 1.73 (m, 2H), 1.51 (m, 4H). The head-to-tail ratio was determined as >97% by ^{1}H NMR. M_n = 31600, and M_w/M_n = 1.30 as determined by GPC.

Poly[3-(6-iodohexyl)thiophene] (7). Polymer **6** (137 mg), $[CH_3(CH_2)_3]_4NBr$ (120 mg, 0.37 mmol) and 40 mL of toluene were added to a two-necked 100 mL round-bottom flask equipped with a stirring bar. KI solution (3.0 g, 18 mmol in 20 mL of water) was then added into the flask, and the solution was heated to reflux for two days. The organic layer was extracted with toluene, and the solution was concentrated by evaporation. The solution was subsequently precipitated into a MeOH solution and filtered. This precipitation procedure was repeated twice, and the solid residue was dried under vacuum to give the product **7** (152 mg) in 93% yield.

^{1}H NMR (500 MHz, $CDCl_3$): 6.98 (s, 1H), 3.23 (t, 2H), 2.83 (t, 2H), 1.88 (m, 2H), 1.73 (m, 2H), 1.51 (m. 4H). M_n = 34600, and M_w/M_n = 1.34 as determined by GPC.

Poly[3-(5-hexenyl)thiophene] (P3HNT). 7 (178 mg) and 35 mL of THF were added to a two-necked 100 mL round-bottom flask equipped with a stirring bar. The solution was heated in order to dissolve the polymer completely. After cooling the flask to room temperature, *t*-BuOK (1.0 M in THF, 12.2 mL, 12.2 mmol) was added with a syringe. After the solution was stirred for 8 h at room temperature, the mixture was quenched into MeOH. After filtration, the polymer was dissolved into $CHCl_3$ and washed twice with water. The organic layer was extracted and concentrated by evaporation, and the residual solution was precipitated into MeOH again. The solution was then filtrated, and the residue was dried in vacuum to give P3HNT (90 mg) in 90% yield.

^{1}H NMR (500 MHz, $CDCl_3$): 6.98 (s, 1H), 5.88−5.80 (m, 1H), 5.05−4.96 (dd, 2H), 2.82 (t, 2H), 2.13 (m, 2H), 1.73 (m, 2H), 1.53 (m, 2H). M_n = 27900, and M_w/M_n = 1.47 as determined by GPC.

Measurements. Gel permeation chromatography (GPC) was performed on a Shimadzu Prominence system equipped with a UV detector using $CHCl_3$ as the eluent at 40 °C. The sample solutions were filtered with a PTFE filter (pore size: 0.2 μm) before injection. The ^{1}H NMR spectra were measured on a JEOL Alpha FT-NMR spectrometer equipped with an OXFORD superconducting magnet system (500 MHz). Furthermore, the UV−vis spectra and the FT-IR spectra were recorded on a JASCO V-650 spectrophotometer and IR Prestige-21 systems (Shimadzu), respectively. The FT-IR sample was prepared by drop-casting of polymer solution onto KBr substrate and annealed in situ under N_2 flow at 150 °C. The measurements were conducted at room temperature. Differential scanning calorimetry (DSC) was performed on Rigaku DSC 8230 with a heating rate of 5 K min^{-1} under N_2 flow. X-ray diffraction (XRD) patterns were recorded on a Rigaku RCD-2400H diffractometer, and photoelectron yield spectroscopy (PYS) was recorded on an AC-3 photoelectron spectroscopy in air (Riken Keiki Co., Ltd.) with the samples spin-coated onto ITO substrates. The surface of the organic layers and the devices were observed using a Nikon polarization microscope LV 100TP-12.

Film Preparation for UV Spectra. The pristine films of P3HNT and P3HT and the polymer:PCBM mixture films were prepared by the conventional spin-coating technique from a chlorobenzene solution (12 mg mL^{-1} for the polymer films and 12 mg mL^{-1} of the polymer and 9.6 mg mL^{-1} of PCBM for the mixture films) at room temperature. A quartz plate was used as a substrate for the spin coating after being washed by ultrasonication sequentially in the detergent solution, water, and acetone. The polymer films were dried under nitrogen for 10 min after the spin-coating was completed, and subsequently annealed for 5 min.

The films for the evaluation of the cross-linking property were prepared by the same method. The pristine films, the polymer, and PCBM mixutured films were prepared using a chlorobenzene

solution (10 mg mL^{-1} for the polymer films, 10 mg mL^{-1} of the polymer, and 8 mg mL^{-1} of PCBM for the mixture films).

Device Preparation. Organic photovoltaic cells (PV cells) were prepared with the structure of ITO/PEDOT:PSS/active layer/Al. The ITO-coated glass substrates were washed by ultrasonication sequentially in detergent, water, acetone, and 2-propanol. PEDOT:PSS was spin-coated on the ITO substrate at 3000 rpm. After drying the substrates under vacuum at 140 °C for 30 min, they were transferred into the glovebox. All of the following procedures (except the measurements of the device performance) were conducted inside the glovebox.

The polymer (12 mg mL^{-1}) and PCBM (9.6 mg mL^{-1}) were dissolved into chlorobenzene at 40 °C by stirring for several hours. After filtration with a PTFE filter (0.2 μm), the solution was spin-coated on the substrate at 600 rpm. After drying the chlorobenzene, the substrate was transferred into an evaporation chamber (ALS technology H-2807 vacuum evaporation system with E-100 load lock). An Al electrode (80 nm) was evaporated onto the substrate under high vacuum ($10^{-4}-10^{-5}$ Pa). After the deposition, the device was thermally annealed on a hot plate. The measurements were conducted under the irradiation of AM 1.5 simulated solar light (100 mW cm^{-2}, Peccell Technologies PCE-L11). The irradiated area of the device was defined with a photo mask as 0.06 cm^2. The current−voltage characteristics of the photovoltaic cells were measured using the Keithley 2400 $I-V$ measurement system. The light intensity was adjusted with a standard silicon solar cell and an optical filter (Bunkou Keiki BS520).

Acknowledgment. We thank Prof. Kubo (The University of Tokyo) for the PYS measurements, as well as Mr. Qingshuo Wei for the P3HT synthesis. This work is supported in part by Tokuyama Science Foundation.

Supporting Information Available: Text describing the synthesis and figures showing the UV−vis, PYS, ^{1}H NMR and GPC traces of the polymers and AFM images of the blend film surface. This material is available free of charge via the Internet at http://pubs.acs.org.

References and Notes

(1) Giovanella, U.; Pasini, M.; Destri, S.; Porzio, W.; Botta, C. *Synth. Met.* **2008**, *158*, 113–119.
(2) Wu, F. I.; Dodda, R.; Reddy, D. S.; Shu, C. F. *J. Mater. Chem.* **2002**, *12*, 2893–2897.
(3) Grozea, D.; Turak, A.; Yuan, Y.; Han, S.; Lu, Z. H.; Kim, W. Y. *J. Appl. Phys.* **2007**, 101.
(4) Schuller, S.; Schilinsky, P.; Hauch, J.; Brabec, C. J. *Appl. Phys. A-Mater. Sci. Process.* **2004**, *79*, 37–40.
(5) Kroon, J. M.; Wienk, M. M.; Verhees, W. J. H.; Hummelen, J. C. *Thin Solid Films* **2002**, *403*, 223–228.
(6) Park, D. K.; Chun, A. R.; Kim, S. H.; Kim, M. S.; Kim, C. G.; Kwon, T. W.; Cho, S. J.; Woo, H. S.; Lee, J. G.; Lee, S. H.; Guo, Z. X. *Appl. Phys. Lett.* **2007**, 91.
(7) Kim, J. Y.; Lee, K.; Coates, N. E.; Moses, D.; Nguyen, T. Q.; Dante, M.; Heeger, A. J. *Science* **2007**, *317*, 222–225.
(8) Yan, H.; Yoon, M. H.; Facchetti, A.; Marks, T. J. *Appl. Phys. Lett.* **2005**, 87.
(9) Bellmann, E.; Shaheen, S. E.; Thayumanavan, S.; Barlow, S.; Grubbs, R. H.; Marder, S. R.; Kippelen, B.; Peyghambarian, N. *Chem. Mater.* **1998**, *10*, 1668–1676.
(10) Liu, S.; Jiang, X. Z.; Ma, H.; Liu, M. S.; Jen, A. K. Y. *Macromolecules* **2000**, *33*, 3514–3517.
(11) Li, W. J.; Wang, Q. W.; Cui, J.; Chou, H.; Shaheen, S. E.; Jabbour, G. E.; Anderson, J.; Lee, P.; Kippelen, B.; Peyghambarian, N.; Armstrong, N. R.; Marks, T. J. *Adv. Mater.* **1999**, *11*, 730–734.
(12) Bacher, A.; Erdelen, C. H.; Paulus, W.; Ringsdorf, H.; Schmidt, H. W.; Schuhmacher, P. *Macromolecules* **1999**, *32*, 4551–4557.
(13) Bayerl, M. S.; Braig, T.; Nuyken, O.; Muller, D. C.; Gross, M.; Meerholz, K. *Macromol. Rapid Commun.* **1999**, *20*, 224–228.
(14) Muller, C. D.; Falcou, A.; Reckefuss, N.; Rojahn, M.; Wiederhirn, V.; Rudati, P.; Frohne, H.; Nuyken, O.; Becker, H.; Meerholz, K. *Nature* **2003**, *421*, 829–833.
(15) Cheng, Y. J.; Liu, M. S.; Zhang, Y.; Niu, Y. H.; Huang, F.; Ka, J. W.; Yip, H. L.; Tian, Y. Q.; Jen, A. K. Y. *Chem. Mater.* **2008**, *20*, 413–422.
(16) Bozano, L. D.; Carter, K. R.; Lee, V. Y.; Miller, R. D.; DiPietro, R.; Scott, J. C. *J. Appl. Phys.* **2003**, *94*, 3061–3068.
(17) Li, Y. N.; Ding, J. F.; Day, M.; Tao, Y.; Lu, J. P.; D'Iorio, M. *Chem. Mater.* **2003**, *15*, 4936–4943.
(18) Yang, C. H.; Hou, J. H.; Zhang, B.; Zhang, S. Q.; He, C.; Fang, H.; Ding, Y. Q.; Ye, J. P.; Li, Y. F. *Macromol. Chem. Phys.* **2005**, *206*, 1311–1318.
(19) Wu, G. L.; Yang, C. H.; Fan, B. H.; Zhang, B.; Chen, X. M.; Li, Y. F. *J. Appl. Polym. Sci.* **2006**, *100*, 2336–2342.
(20) Hiramoto, M.; Fujiwara, H.; Yokoyama, M. *Appl. Phys. Lett.* **1991**, *58*, 1062–1064.
(21) Yu, G.; Gao, J.; Hummelen, J. C.; Wudl, F.; Heeger, A. J. *Science* **1995**, *270*, 1789–1791.
(22) Hoppe, H.; Sariciftci, N. S. *J. Mater. Chem.* **2006**, *16*, 45–61.
(23) Li, G.; Shrotriya, V.; Huang, J. S.; Yao, Y.; Moriarty, T.; Emery, K.; Yang, Y. *Nat. Mater.* **2005**, *4*, 864–868.
(24) Campoy-Quiles, M.; Ferenczi, T.; Agostinelli, T.; Etchegoin, P. G.; Kim, Y.; Anthopoulos, T. D.; Stavrinou, P. N.; Bradley, D. D. C.; Nelson, J. *Nat. Mater.* **2008**, *7*, 158–164.
(25) Padinger, F.; Rittberger, R. S.; Sariciftci, N. S. *Adv. Funct. Mater.* **2003**, *13*, 85–88.
(26) Ma, W. L.; Yang, C. Y.; Gong, X.; Lee, K.; Heeger, A. J. *Adv. Funct. Mater.* **2005**, *15*, 1617–1622.
(27) Bertho, S.; Haeldermans, I.; Swinnen, A.; Moons, W.; Martens, T.; Lutsen, L.; Vanderzande, D.; Manca, J.; Senes, A.; Bonfiglio, A. *Sol. Energy Mater. Sol. Cells* **2007**, *91*, 385–389.
(28) Swinnen, A.; Haeldermans, I.; Vanlaeke, P.; D'Haen, J.; Poortmans, J.; D'Olieslaeger, M.; Manca, J. V. *Eur. Phys. J. Appl. Phys.* **2006**, *36*, 251–256.
(29) Sivula, K.; Luscombe, C. K.; Thompson, B. C.; Frechet, J. M. J. *J. Am. Chem. Soc.* **2006**, *128*, 13988–13989.
(30) Sivula, K.; Ball, Z. T.; Watanabe, N.; Frechet, J. M. J. *Adv. Mater.* **2006**, *18*, 206–210.
(31) Woo, C. H.; Thompson, B. C.; Kim, B. J.; Toney, M. F.; Frechet, J. M. J. *J. Am. Chem. Soc.* **2008**, *130*, 16324–16329.
(32) Padinger, F.; Fromherz, T.; Denk, P.; Brabec, C. J.; Zettner, J.; Hierl, T.; Sariciftci, N. S. *Synth. Met.* **2001**, *121*, 1605–1606.
(33) Bertho, S.; Janssen, G.; Cleij, T. J.; Conings, B.; Moons, W.; Gadisa, A.; D'Haen, J.; Goovaerts, E.; Lutsen, L.; Manca, J.; Vanderzande, D. *Sol. Energy Mater. Sol. Cells* **2008**, *92*, 753–760.
(34) Zhu, Z.; Hadjikyriacou, S.; Waller, D.; Gaudiana, R. *J. Macromol. Sci. Pure and Appl. Chem.* **2004**, *A41*, 1467–1487.
(35) Drees, M.; Hoppe, H.; Winder, C.; Neugebauer, H.; Sariciftci, N. S.; Schwinger, W.; Schaffler, F.; Topf, C.; Scharber, M. C.; Zhu, Z. G.; Gaudiana, R. *J. Mater. Chem.* **2005**, *15*, 5158–5163.
(36) Zhang, Y.; Tajima, K.; Hirota, K.; Hashimoto, K. *J. Am. Chem. Soc.* **2008**, *130*, 7812–7813.
(37) Thompson, B. C.; Kim, B. J.; Kavulak, D. F.; Sivula, K.; Mauldin, C.; Frechet, J. M. J. *Macromolecules* **2007**, *40*, 7425–7428.
(38) Tajima, K.; Suzuki, Y.; Hashimoto, K. *J. Phys. Chem. C* **2008**, *112*, 8507–8510.
(39) Zhai, L.; Pilston, R. L.; Zaiger, K. L.; Stokes, K. K.; McCullough, R. D. *Macromolecules* **2003**, *36*, 61–64.
(40) Bauerle, P.; Wurthner, F.; Heid, S. *Angew. Chem., Int. Ed. Engl.* **1990**, *29*, 419–420.
(41) Miyakoshi, R.; Yokoyama, A.; Yokozawa, T. *Macromol. Rapid Commun.* **2004**, *25*, 1663–1666.
(42) Trznadel, M.; Pron, A.; Zagorska, M. *Macromolecules* **1998**, *31*, 5051–5058.
(43) Loewe, R. S.; Khersonsky, S. M.; McCullough, R. D. *Adv. Mater.* **1999**, *11*, 250–253.
(44) Brown, P. J.; Thomas, D. S.; Kohler, A.; Wilson, J. S.; Kim, J. S.; Ramsdale, C. M.; Sirringhaus, H.; Friend, R. H. *Phys. Rev. B* **2003**, *67*, 16.
(45) Zen, A.; Saphiannikova, M.; Neher, D.; Grenzer, J.; Grigorian, S.; Pietsch, U.; Asawapirom, U.; Janietz, S.; Scherf, U.; Lieberwirth, I.; Wegner, G. *Macromolecules* **2006**, *39*, 2162–2171.
(46) Kline, R. J.; McGehee, M. D.; Kadnikova, E. N.; Liu, J. S.; Frechet, J. M. J.; Toney, M. F. *Macromolecules* **2005**, *38*, 3312–3319.
(47) Brabec, C. J.; Cravino, A.; Meissner, D.; Sariciftci, N. S.; Fromherz, T.; Rispens, M. T.; Sanchez, L.; Hummelen, J. C. *Adv. Funct. Mater.* **2001**, *11*, 374–380.
(48) Gadisa, A.; Svensson, M.; Andersson, M. R.; Inganas, O. *Appl. Phys. Lett.* **2004**, *84*, 1609–1611.
(49) Scharber, M. C.; Wuhlbacher, D.; Koppe, M.; Denk, P.; Waldauf, C.; Heeger, A. J.; Brabec, C. L. *Adv. Mater.* **2006**, *18*, 789–794.
(50) Swinnen, A.; Haeldermans, I.; vande Ven, M.; D'Haen, J.; Vanhoyland, G.; Aresu, S.; D'Olieslaeger, M.; Manca, J. *Adv. Funct. Mater.* **2006**, *16*, 760–765.

MA802839A